Degree-one mantle convection: Dependence on internal heating and temperature-dependent rheology

Allen K. McNamara[1] and Shijie Zhong

Department of Physics, University of Colorado, Boulder, Colorado, USA

[1] Geophysical and geological observations suggest that a degree-one mantle flow pattern, consisting of one upwelling and one downwelling, may have existed at some time in the mantles of Mars, the Moon, and perhaps even for the Earth during times of supercontinent formation. Simple fluid experiments utilizing isoviscous rheologies predict shorter wavelength flow patterns, and it is therefore important to determine fluid dynamical parameter sets which lead to larger wavelength flow patterns consistent with observations. We perform a series of numerical fluid dynamics calculations in a spherical 3-D geometry in which we vary Rayleigh number, rheological activation parameter, and the degree of internal heating in order to define which parameter choices can lead to degree-one mantle convection. We find that increasing the degree of internal heating increases the interior temperature of the mantle which leads to a larger viscosity contrast across the top thermal boundary layer, and that degree-one mantle flow occurs only in cases which exhibit internal heating, utilize activation coefficients which lead to 10^3 or higher viscosity contrasts across the mantle, and have viscosity contrasts across the top thermal boundary layer within the range of $200-3000$. **Citation:** McNamara, A. K., and S. Zhong (2005), Degree-one mantle convection: Dependence on internal heating and temperature-dependent rheology, *Geophys. Res. Lett.*, *32*, L01301, doi:10.1029/2004GL021082.

1. Introduction

[2] Seismic tomography models [e.g., *Masters et al.*, 1996; *Grand et al.*, 1997] are characterized by long-wavelength heterogeneity in the Earth's present-day mantle, likely associated with plate tectonics [*Davies*, 1988; *Bunge et al.*, 1998; *Lithgow-Bertelloni and Richards*, 1998].

[3] This long-wavelength behavior is not limited to the Earth; the surface geology of the Moon and Mars hints at an early degree-one mantle flow structure (consisting of one upwelling and one downwelling) resulting in the well-observed hemispherical crustal dichotomy and the Tharsis Rise on Mars [*Wise et al.*, 1979; *Harder and Christensen*, 1996] and the hemispherical Mare basalts distribution on the Moon [*Stevenson*, 1980; *Zhong et al.*, 2000a]. Moreover, the formation of supercontinents on the Earth hints that even longer wavelength flow structure than those observed today may have once existed in the past. Degree-one mantle flow is an intriguing possibility given that it represents the longest possible flow wavelength.

[4] These observations are in contrast to simple Boussinesq isoviscous fluid dynamical experiments however, which exhibit much smaller wavelength flow patterns [*Schubert et al.*, 1990] than that observed on Earth or inferred for the early history of Mars. Considerable effort has been put forth to understand the physics behind generating larger wavelength flow patterns than those observed in simple experiments.

[5] A fundamental question is whether observed large wavelength mantle flow results from the complicated brittle-elastic physics of the lithosphere or whether the material properties of the mantle (i.e., rheology, phase transitions, chemical heterogeneity) are the cause.

[6] It has been shown that the presence of continents or rigid plates can organize mantle flow into larger wavelengths [*Davies*, 1988; *Gurnis and Zhong*, 1991; *Zhong and Gurnis*, 1993], however these studies treat plates or continents as stiff rafts with sizes independent of deeper mantle forces.

[7] Degree-one convection may occur if the planetary core is relatively small, as supposed by *Zhong et al.* [2000a] for the Moon. However, for other terrestrial bodies with a larger core, different mechanisms are needed. Numerical modeling incorporating phase transitions have been shown to increase flow wavelength for parameters relevant to Earth [*Tackley et al.*, 1993, 1994; *Tackley*, 1996] and produce degree-one flow for those conditions possibly relevant to Mars [*Breuer et al.*, 1998; *Harder and Christensen*, 1996; *Harder*, 2000].

[8] Numerical models also show that depth-dependent viscosity plays a role in increasing flow wavelength [*Bunge et al.*, 1996; *Tackley*, 1996; *Zhong and Zuber*, 2001]. Using a linear stability analysis, *Zhong and Zuber* [2001] examined the physical causes of increased wavelengths from depth-dependent viscosity. With 2-D spherically axisymmetrical models of mantle convection with strongly temperature-dependent viscosity, *Zhong and Zuber* [2001] found that degree-one flow structure could be achieved if the asthenosphere was significantly weaker than the lower mantle. *Harder* [2000] observed degree-one flow structure for lithospheric radial viscosity (no temperature-dependence) contrasts of 10^3, even without the presence of an endothermic phase transition near the base of the mantle.

[9] *Ratcliff et al.* [1996, 1997] examined the effect of temperature-dependent rheology on the planform of spherical convection. As the activation parameter was increased from that leading to a 'mobile lid' to that leading to a 'sluggish lid' for a Rayleigh number of 10^5, convection

---

[1]Now at Department of Geological Sciences, Arizona State University, Tempe, Arizona, USA.

Table 1. Input Parameters and Output

	Input Parameters				Output-Snapshot Characteristics					
Case	Ra_{input}	A	$\Delta\eta$	H	Ra_{eff}	$\Delta\eta_{lith}$	$\langle T \rangle$	$\langle \eta \rangle$	%Internal	Strongest Degree(s)
1	4.56×10^5	6.908	10^3	0	1.3×10^5	11	0.32	3.47	0	4
2	4.56×10^5	6.908	10^3	50	2.4×10^6	327	0.74	0.19	63	1
3	4.56×10^5	6.908	10^3	100	8.3×10^6	1129	0.92	0.05	82	1
4	9.11×10^5	6.908	10^3	0	4.3×10^5	18	0.39	2.14	0	2,3,4
5	9.11×10^5	6.908	10^3	50	3.9×10^6	230	0.71	0.23	58	1
6	9.11×10^5	6.908	10^3	100	1.3×10^7	799	0.88	0.07	78	1
7	4.56×10^6	6.908	10^3	50	1.5×10^7	145	0.67	0.31	55	5,6
8	4.56×10^6	6.908	10^3	100	3.9×10^7	331	0.79	0.13	70	1,2,3,4
9	4.56×10^5	4.605	10^2	50	1.1×10^6	35	0.70	0.40	65	6,8,9,12,13
10	4.56×10^5	9.210	10^4	0	6.6×10^5	231	0.54	0.69	0	12
11	4.56×10^5	9.210	10^4	50	6.0×10^6	2972	0.78	0.08	64	1

Ra_{input} is the input Rayleigh number, A is the activation parameter, $\Delta\eta$ is the viscosity contrast across the entire model, H is the non-dimensional internal heating, Ra_{eff} is the effective Rayleigh number (input Rayleigh number over average viscosity), $\Delta\eta_{lith}$ is the viscosity contrast over the top thermal boundary layer, $\langle T \rangle$ is the volume averaged temperature, $\langle \eta \rangle$ is the log-volume averaged viscosity, % internal is the percentage of total heat loss attributed to internal heating, and strongest degree(s) indicates which wavelengths dominate the flow pattern. If multiple degrees are shown, this indicates that multiple degrees dominate with similar power.

patterns took on considerably longer wavelength flow patterns. Although they do not report any results with degree-one flow, they do observe long-wavelength degree-two flow patterns.

[10] In this work, we focus on examining the effect that temperature-dependent rheology, internal heating, and Rayleigh number have on whether convection develops a degree-one flow pattern. We find that for activation parameters which lead to mantle viscosity contrasts of 10^3 and 10^4, degree-one flow occurs only for cases in which internal heating is applied. This result is only valid for a limited range of effective Rayleigh numbers.

2. Model Setup

[11] The numerical calculations are performed by solving the non-dimensional conservation equations of mass, momentum, and energy in the Boussinesq approximation using the 3D spherical finite element code CitcomS as outlined by *Zhong et al.* [2000b]. Isothermal temperature and free-slip velocity boundary conditions are employed at the top and bottom boundaries with non-dimensional radii of 1.0 and 0.55, respectively. The model domain is comprised of ~1.3 million elements (49 × 49 × 49 for each of the 12 caps comprising the sphere). Length is nondimensionalized by the planetary radius, however the Rayleigh number is defined by mantle thickness as follows:

$$Ra = \frac{\alpha\rho g \Delta T h^3}{\eta\kappa}, \qquad (1)$$

where α, ρ, g, ΔT, h, and κ are the thermal expansivity, density, acceleration of gravity, temperature drop across the mantle, mantle thickness, and thermal diffusivity. η_o is the reference viscosity, defined as the viscosity at non-dimensional temperature $T = 0.5$.

[12] The non-dimensional temperature-dependent viscosity is given as:

$$\eta(T) = \exp(A(0.5 - T)) \qquad (2)$$

where A is the activation parameter which controls the temperature-dependence of viscosity. The amount of

internal heating is controlled by the non-dimensional heat production rate, H, defined as:

$$H = \frac{QR_o^2}{\rho c_p \kappa \Delta T} \qquad (3)$$

where Q, R_o, and c_p are the volumetric heat production, planetary radius, and specific heat, respectively.

[13] The initial condition for each case is a radial temperature profile derived from steady-state results of 2D spherically axisymmetric calculations. We run each 3-D calculation until a quasi steady-state convection pattern is established.

3. Results

[14] We performed 11 calculations in which we varied the amount of internal heating, the activation parameter (A), and input Rayleigh number (Ra). A was varied in order to lead to 10^2, 10^3, and 10^4 viscosity contrasts across the entire mantle. (Table 1) We examined the pattern of flow as inferred from the temperature field both qualitatively from residual temperature plots and quantitatively from power spectra. We also calculated the viscosity contrast across the top thermal boundary layer ($\Delta\eta_{lith}$), the volume-averaged temperature ($\langle T \rangle$), the percentage of total heat loss attributed to internal heating, and the log-volume-averaged viscosity ($\langle \eta \rangle$) which is the exponential of the volume-averaged logarithm of viscosity (performed so that the average is not overly biased by the high viscosity regions). The effective Rayleigh number (Ra_{eff}) of each case is calculated by dividing Ra by $\langle \eta \rangle$. These quantities are also displayed in Table 1.

[15] Figures 1a and 2a show the residual temperature field and radial power spectra, respectively, from Case 1 with $Ra = 4.56 \times 10^5$ which lacks internal heating and has an A which leads to 10^3 viscosity contrast across the entire mantle. The parameters used in this case clearly lead to a well-organized convection pattern dominated by a degree-four wavelength. For this case, $\langle T \rangle = 0.32$, $\langle \eta \rangle = 3.47$, and $Ra_{eff} = 1.3 \times 10^5$ (Table 1).

[16] Figures 1b and 2b show results from Case 2 which differs from Case 1 only by the addition of internal heating.
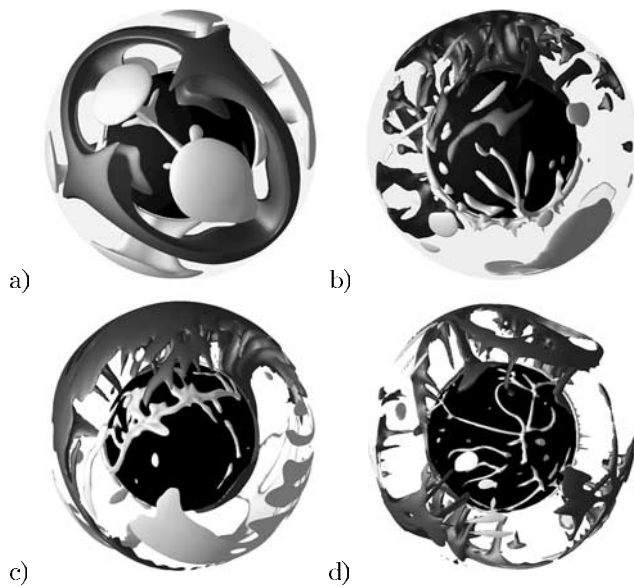
Figure 1. Isosurfaces of residual temperature. Dark and light surfaces represent the −0.15 (cold) and +0.15 (hot) contours, respectively, where 0 is defined as the average temperature for the given radius. (a) Case 1 (b) Case 2 (c) Case 6 (d) Case 8.

The addition of internal heating increases $\langle T \rangle$, and as a consequence, $\langle \eta \rangle$ is reduced and Ra_{eff} is increased (i.e., $\langle T \rangle = 0.74$, $\langle \eta \rangle = 0.19$, and $Ra_{eff} = 2.4 \times 10^6$). $\Delta\eta_{lith} = 327$ which is roughly 30 times greater than that of Case 1. Both the residual temperature and spectral plots reveal that most of the power in Case 2 is in degree-one. Doubling the amount of internal heating (Case 3) leads to similar degree-one structure. Note that in Case 3, the mantle temperature immediately below the top thermal boundary layer is slightly larger than unity due to the high amount of internal heating which leads to a somewhat higher $\Delta\eta_{lith}$ than that across the mantle (Table 1).

[17] We performed another series of calculations similar to Cases 1−3 but with higher Ra. We find that with no internal heating (Case 4), degree-one structure fails to form, and most of the power is in degrees 2−4, similar to Case 1 with no internal heating. The addition of internal heating (Cases 5 and 6) acts to increase $\Delta\eta_{lith}$, and degree-one structure forms as is observed in the lower Ra number cases (Cases 2 and 3). Figures 1c and 2c show results from Case 6. Ra_{eff} for this case is 1.3×10^7 which is significantly higher than that used by *Ratcliff* [1996, 1997] and *Harder* [2000]. Again, the dominant mode of flow is degree-one.

[18] We performed two internal heating calculations (Cases 7 and 8) comparable to Cases 5 and 6, respectively, but with even greater Ra. Degree-one structure fails to dominate the flow pattern in these cases. Most of the power in Case 7 is in degrees 5 and 6. Figures 1d and 2d show results from Case 8 which exhibits twice the amount of internal heating as Case 7. Although there is a strong degree-one signature at the base of the mantle, power is spread relatively equally with higher degrees, and degrees 1−4 have similar power.

[19] We performed a calculation, Case 9, which is similar to Case 2 except for A, leading to a lower viscosity contrast

of 10^2 across the mantle. Compared to Case 2, $\Delta\eta_{lith}$ is significantly reduced and is more similar to that of Case 1 which lacks internal heating. In this case, shorter wavelength structures (degrees 6−13) dominate the flow pattern, whereas degree-one structure dominates in Case 2.

[20] Cases 10 and 11 were performed with higher A leading to a 10^4 viscosity contrast across the mantle, but are otherwise identical to cases 1 and 2, respectively. Case 10 lacks internal heating and does not develop a degree-one flow structure similar to Case 1. Case 11, on the other hand, includes internal heating and does develop a degree-one flow structure, similar to that in Case 2.

4. Discussion and Conclusions

[21] A summary of results is given in Figure 3 in which both $\Delta\eta_{lith}$ (Figure 3a) and $\langle T \rangle$ (Figure 3b) are plotted against Ra_{eff}. See caption for Figure 3 for a description of the symbols.

[22] We find that for a given set of parameters, as internal heating is increased, $\langle T \rangle$ increases, and as a result, a greater percentage of the total viscosity contrast takes place across the top thermal boundary layer (compare Cases 1 and 2). We also find that the greater efficiency of cooling associated with higher Ra leads to lower $\langle T \rangle$ and consequently, lower $\Delta\eta_{lith}$ (compare Cases 2 and 5).

[23] For the parameters studied here, degree-one mantle convection fails to form for cases without internal heating. It is initially tempting to attribute the development of degree-one mantle convection to a given minimum $\Delta\eta_{lith}$, however, we find that this relationship is more complicated. The lowest $\Delta\eta_{lith}$ associated with degree-one convection is 230 (in Case 5). Case 10, with no internal heating but higher A, exhibits a similar viscosity contrast, however, the strongest power of convection is in degree 12. Case 8, with the
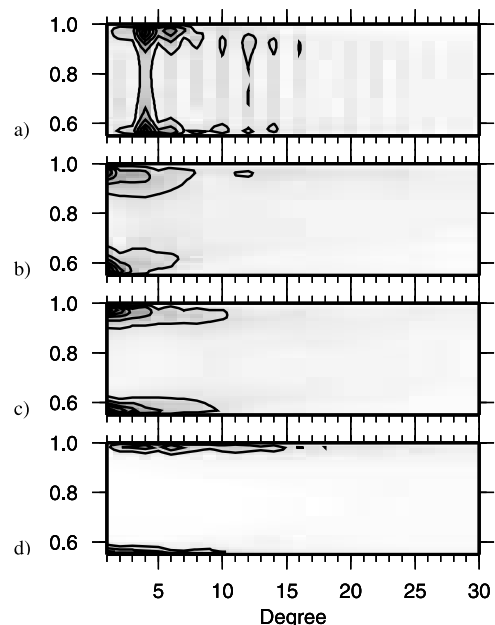
Figure 2. Radial dependence on the power spectrum derived from the temperature field. Darker colors represent higher power. Degree 1 is the lowest value on the axis. (a) Case 1 (b) Case 2 (c) Case 6 (d) Case 8.
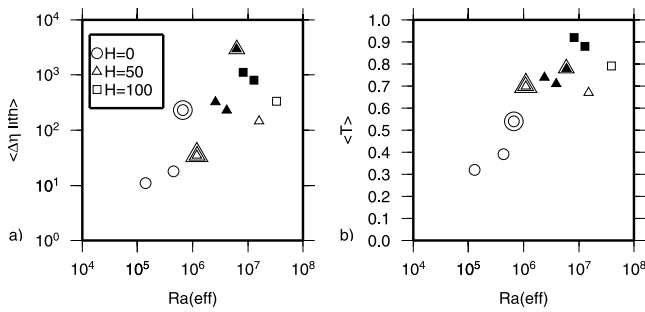
Figure 3. (a) $\Delta\eta_{lith}$ versus Ra_{eff}, and (b) $\langle T \rangle$ versus Ra_{eff} for all cases. The amount of internal heating is represented by symbol type. Circles, triangles, and squares represent cases with 0, 50, and 100 internal heating, respectively. Filled symbols represent cases in which degree-one dominates the mantle flow pattern. The viscosity contrast across the system is represented by symbol borders; symbols with 1, 2, and 3 borders represent cases with 10^3, 10^4, and 10^2 viscosity contrasts, respectively.

maximum Ra_{eff} in our calculations, has an even higher $\Delta\eta_{lith}$ than Case 5 yet does not develop predominantly degree-one convection. This indicates that both Ra_{eff} and $\Delta\eta_{lith}$ play a role in forming degree-one convection.

[24] It is not straightforward from Figure 3 to discover a relationship between degree-one mantle convection, $\Delta\eta_{lith}$, $\langle T \rangle$, Ra_{eff}, and A. We find that cases that develop degree-one convection have $\Delta\eta_{lith}$ spanning the range $\sim 200{-}3000$, however, not all calculations within this range lead to degree-one convection. Instead, we propose that a given $\Delta\eta_{lith}$ likely is a prerequisite for degree-one mantle convection.

[25] The idea that $\Delta\eta_{lith}$ may contribute to degree-one convection is not unfounded. From 3-D spherical models with strictly depth-dependent viscosity (i.e., no temperature-dependence), *Harder* [2000] found that processes that influence the boundary layers may have a strong influence on the flow wavelength. He found that degree-one may form for a moderate (10^3) $\Delta\eta_{lith}$, but much larger contrasts may prevent degree-one. Our models with temperature-dependent viscosity are consistent with his results.

[26] Although this work is not too dissimilar than that of *Ratcliff et al.* [1996, 1997], we report results not observed in their work and explore a larger parameter space. For A leading to 10^3 viscosity contrasts across the mantle, they observe that degree-two dominates the flow pattern, and they do not mention the development of degree-one convection in any of their calculations. It appears that Rayleigh numbers are slightly higher and internal heating is somewhat lower in our work than in theirs, which may lead to the differences between our studies.

[27] We find that degree-one mantle flow can dominate under certain parameter choices of A, internal heating, and Ra. We suspect that $\Delta\eta_{lith}$ plays an important role in the development of degree-one, although the interplay of parameters probably makes this relationship complicated. Future work will be needed to more carefully differentiate the effects of internal heating from A. Nevertheless, this is the first work that we are aware of in which degree-one mantle convection is formed by using temperature-

dependent rheology alone without radial discontinuities or phase changes in 3-D spherical geometry, and we put forth that the reporting of these observations may contribute to a better understanding of the mechanisms behind the development of degree-one mantle convection.

[28] With the moderately temperature-dependent viscosity, our studies should be applicable to mantle convection with a mobile surface, for example, the plate tectonic style convection for Earth. Although Martian and lunar mantle convection are often considered as a stagnant lid convection, we believe that our results are relevant to the early evolution of these terrestrial bodies. Recently, *Roberts and Zhong* [2004] suggest that a relatively thick crust and the relatively thin elastic plate thickness for early Mars [*Zuber et al.*, 2000] may lead to a mobile mantle lithosphere due to the weak crust channel that decouples the crust and mantle that is relatively hot. If this suggestion is correct, then we believe that our models with moderately temperature-dependent viscosity and mobile lid convection are also relevant to Mars.

References

Breuer, D., D. A. Yuen, T. Spohn, and S. Zhang (1998), Three dimensional models of Martian mantle convection with phase transitions, *Geophys. Res. Lett.*, *25*, 229–232.

Bunge, H.-P., M. A. Richards, and J. R. Baumgardner (1996), Effect of depth-dependent viscosity on the planform of mantle convection, *Nature*, *379*, 436–438.

Bunge, H.-P., M. A. Richards, C. Lithgow-Bertelloni, J. R. Baumgardner, S. P. Grand, and B. A. Romanowicz (1998), Timescales and heterogeneous structure in geodynamic Earth models, *Science*, *280*, 91–95.

Davies, G. F. (1988), Role of the lithosphere in mantle convection, *J. Geophys. Res.*, *93*, 10,451–10,466.

Grand, S. P., R. D. van der Hilst, and S. Widiyantoro (1997), Global seismic tomography: A snapshot of convection in the Earth, *Geol. Soc. Am. Today*, *7*, 1–7.

Gurnis, M., and S. Zhong (1991), Generation of long wavelength heterogeneity in the mantle by the dynamic interaction between plates and convection, *Geophys. Res. Lett.*, *18*, 581–584.

Harder, H. (2000), Mantle convection and the dynamic geoid of Mars, *Geophys. Res. Lett.*, *27*, 301–304.

Harder, H., and U. Christensen (1996), A one-plume model of Martian mantle convection, *Nature*, *380*, 507–509.

Lithgow-Bertelloni, C., and M. A. Richards (1998), The dynamics of Cenozoic and Mesozoic plate motions, *Rev. Geophys.*, *36*, 27–78.

Masters, G., S. Johnson, G. Laske, and H. Bolton (1996), A shear-velocity model of the mantle, *Philos. Trans. R. Soc. London, Ser. A*, *354*, 1385–1411.

Ratcliff, J. T., G. Schubert, and A. Zebib (1996), Effects of temperature-dependent viscosity on thermal convection in a spherical shell, *Physica D*, *97*, 242–252.

Ratcliff, J. T., P. J. Tackley, G. Schubert, and A. Zebib (1997), Transitions in thermal convection with strongly variable viscosity, *Phys. Earth Planet. Inter.*, *102*, 201–212.

Roberts, J. H., and S. Zhong (2004), Degree-1 mantle convection as a process for generating the Martian hemispheric dichotomy, paper presented at Workshop on Hemispheres Apart: The origin and Modification of the Martian Crustal Dichotomy, Lunar and Planet. Inst., Houston.

Schubert, G., D. Bercovici, and G. A. Glatzmaier (1990), Mantle dynamics in Mars and Venus: Influences of an immobile lithosphere on three-dimensional mantle convection, *J. Geophys. Res.*, *95*, 14,105–14,129.

Stevenson, D. J. (1980), Lunar symmetry and paleomagnetism, *Nature*, *287*, 520–521.

Tackley, P. J. (1996), On the ability of phase transitions and viscosity layering to induce long wavelength heterogeneity in the mantle, *Geophys. Res. Lett.*, *23*, 1985–1988.

Tackley, P. J., D. J. Stevenson, G. A. Glatzmaier, and G. Schubert (1993), Effects of an endothermic phase transition at 670 km depth

in a spherical model of convection in the Earth's mantle, *Nature*, *361*, 699–704.

Tackley, P. J., D. J. Stevenson, G. A. Glatzmaier, and G. Schubert (1994), Effects of multiple phase transitions in a three-dimensional spherical model of convection in the Earth's mantle, *J. Geophys. Res.*, *99*, 15,877–15,901.

Wise, D. U., M. P. Golombek, and G. E. McGill (1979), Tectonic evolution of Mars, *J. Geophys. Res.*, *84*, 7934–7939.

Zhong, S., and M. Gurnis (1993), Dynamic feedback between an non-subducting raft and thermal convection, *J. Geophys. Res.*, *98*, 12,219–12,232.

Zhong, S., and M. T. Zuber (2001), Degree-1 mantle convection and the crustal dichotomy on Mars, *Earth Planet. Sci. Lett.*, *190*, 75–84.

Zhong, S., E. M. Parmentier, and M. T. Zuber (2000a), A dynamic origin for global asymmetry of lunar mare basalts, *Earth Planet. Sci. Lett.*, *177*, 131–141.

Zhong, S., M. T. Zuber, L. Moresi, and M. Gurnis (2000b), Role of temperature-dependent viscosity and surface plates in spherical shell models of mantle convection, *J. Geophys. Res.*, *105*, 11,063–11,082.

Zuber, M. T., et al. (2000), Internal structure and early thermal evolution of Mars from Mars Global Surveyor topography and gravity, *Science*, *287*, 1788–1793.

————————————

A. K. McNamara, Department of Geological Sciences, Arizona State University, Box 871404, Tempe, AZ 85287–1404, USA. (allen.mcnamara@asu.edu)

S. Zhong, Department of Physics, University of Colorado, 390 UCB, Boulder, CO 80309–0390, USA.